

**Kinetic measurements of shock wave propagation in a three-dimensional complex (dusty) plasma**

D. Samsonov, G. Morfill, H. Thomas, T. Hagl, and H. Rothermel

*Centre for Interdisciplinary Plasma Science, Max-Planck-Institut für Extraterrestrische Physik, D-85740 Garching, Germany*

V. Fortov, A. Lipaev, V. Molotkov, A. Nefedov, and O. Petrov

*Institute for High Energy Densities, Russian Academy of Sciences, 127412 Moscow, Russia*

A. Ivanov and S. Krikalev

*S. P. Korolev RSC Energia, Korolev 141070, Moscow Region, Russia*

(Received 21 August 2002; revised manuscript received 12 December 2002; published 14 March 2003)

“Complex plasmas” consist of electrons, ions, and charged microparticles. The latter are individually observable, allowing kinetic measurements in plasmas. Using a sudden gas pulse, a traveling perturbation was initiated in such a complex plasma and its propagation, acceleration, and steepening—possibly into a shock was followed. The experiment was performed in the PKE-Nefedov laboratory under microgravity conditions on the international space station, i.e., in a complex plasma cloud with very little stored (potential or free) energy and thus free of, e.g., parametric instabilities. The perturbation front remained remarkably smooth, with a microroughness of the order of the interparticle distance. The observations are presented and interpreted.

DOI: 10.1103/PhysRevE.67.036404

PACS number(s): 52.27.Lw, 52.35.Fp, 52.35.Tc, 96.50.Fm

**I. INTRODUCTION**

Shock waves are discontinuous propagating disturbances, which are characterized by a velocity jump followed by a rise in pressure, temperature, and density. They are well studied in gas dynamics [1], where they are classified as weak and strong depending on the relative increase in pressure behind the front. Shocks are known to propagate in solids [2], where they are studied in connection with impacts and explosions in material science and geophysics. They can be elastic, elastic plastic, and strong according to the damage they make to the media. Shocks were also observed in two-dimensional complex fluids such as granular media in a fluid state [3]. Shock waves exist in plasmas [4]. They are usually produced from high amplitude waves by dissipative processes, the most important being collisions with neutrals, viscosity, and Landau damping [5,6]. Existence of dust-acoustic waves and solitons was first considered in Ref. [7]. Shocks in complex (dusty) plasmas were described theoretically by different authors [8–11]. Dust-ion-acoustic shocks have been observed [12,13] as well as weak V-shaped shocks (Mach cones) [14].

Here we report an observation of a traveling perturbation in a three-dimensional complex (dusty) plasma under microgravity conditions, which propagates into a less dense regime and appears to develop into a dust-acoustic (DA) shock. Dust-acoustic shocks have never been seen before.

**II. THE EXPERIMENT AND ANALYSIS TECHNIQUE**

The experiment was performed on board the international space station (ISS) using the PKE-Nefedov laboratory. The plasma was created by a symmetrically driven parallel plate capacitively coupled radio frequency (rf) discharge. The experimental chamber is shown in Fig. 1. It consisted of two electrodes, 4.2 cm in diameter, separated by 3 cm. The inter-electrode space was illuminated by a laser sheet perpendicular to the electrodes and imaged by two side view video cameras.

We used a wide view video camera (field of view is shown in Fig. 1), which had a resolution of 0.0391 mm/pixel in the horizontal and 0.0372 mm/pixel in the vertical direction. The plasma chamber with the laser, video cameras, rf generator, control electronics, and vacuum system was placed in a container on board of the ISS and connected via a cable to a telescope module. The telescope module recorded all experimental data, which were then brought to the earth for analysis.

For this experiment the plasma chamber was filled with argon gas at 0.97 mbar. Plastic spherical particles 3.4  $\mu\text{m}$  in diameter were injected into the electron-ion plasma to form a

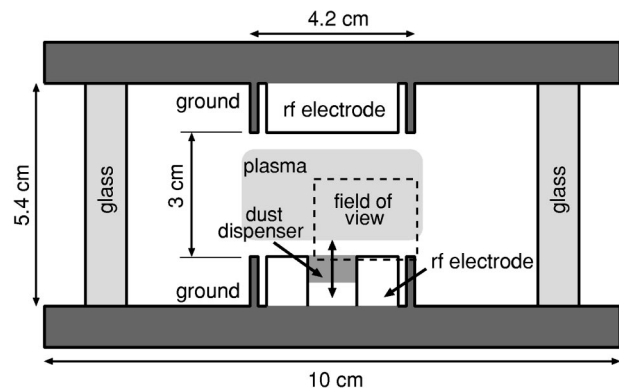


FIG. 1. The side view of the plasma chamber of the PKE-Nefedov experiment. This is a square vacuum chamber, with a size of  $10 \times 10 \text{ cm}^2$ , made of glass. The rf electrodes are flat circular plates, made from stainless steel, with a diameter of 4.2 cm, where a dust dispenser is integrated in the center of each side. The microparticles are injected into the discharge region between the electrodes by an oscillating up and down motion of the dispensers. The particles are accelerated inside the reservoir and released through a sieve with a mesh size slightly larger than the particle diameter. The electrode separation is 3 cm. The excentric field of view of the charge coupled device cameras is shown here with a dashed line.

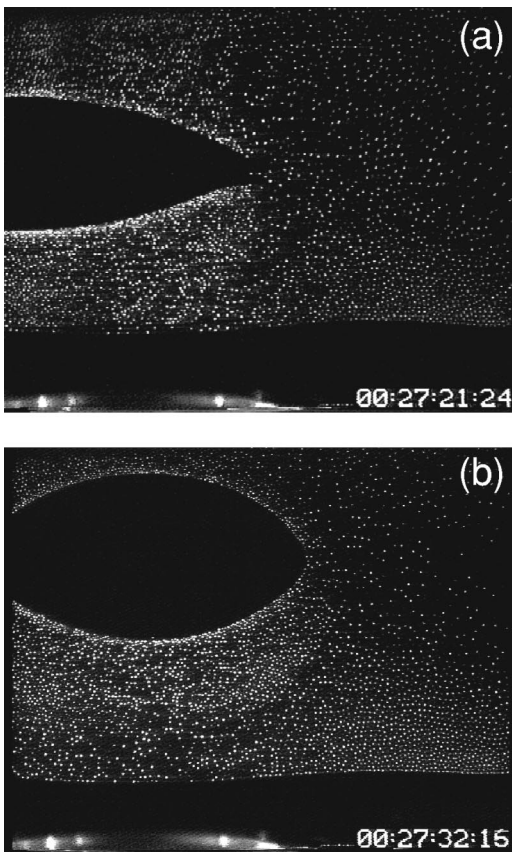


FIG. 2. Field of view ( $30 \times 21.4$  mm) of the video camera. The particles fill up the interelectrode space with the void in the middle. (a) Particle cloud before excitation. The void is slightly shifted down due to the particle motion after the particles were shaken in. (b) Particle cloud after the shock passed and it came to equilibrium. The void is bigger since, first, some particles were lost into the pumping outlet, and second, the gas pressure increased by about 1%.

“complex plasma.” The microspheres were imaged with a side view video camera at 25 interlaced frames per second. The video frames were recorded with a VCR and later digitized and deinterlaced, producing a sequence of images at 50 fps at half the standard vertical resolution ( $768 \times 288$  pixels).

As known from previous experiments under microgravity [15], particles charge up in a plasma and form a cloud between the electrodes with a lentil-shaped void in the center. Figure 2 shows the equilibrium cloud before excitation [Fig. 2(a)] and after the shock passed [Fig. 2(b)]. The particle cloud was in a liquid state in our experiment.

The perturbation was excited by a gas pulse from an electromagnetic valve, which was opened twice for less than a second. This increased the gas pressure by about 1%. The particles were swept from top to bottom by the gas flow, creating a compressional pulse. Figure 3 shows the propagation of the pulse. The traveling perturbation forms in the upper left part of the frame and propagates downward, steepening and speeding up along the way. The front of the perturbation is curved.

We analyzed the frame sequence by identifying the par-

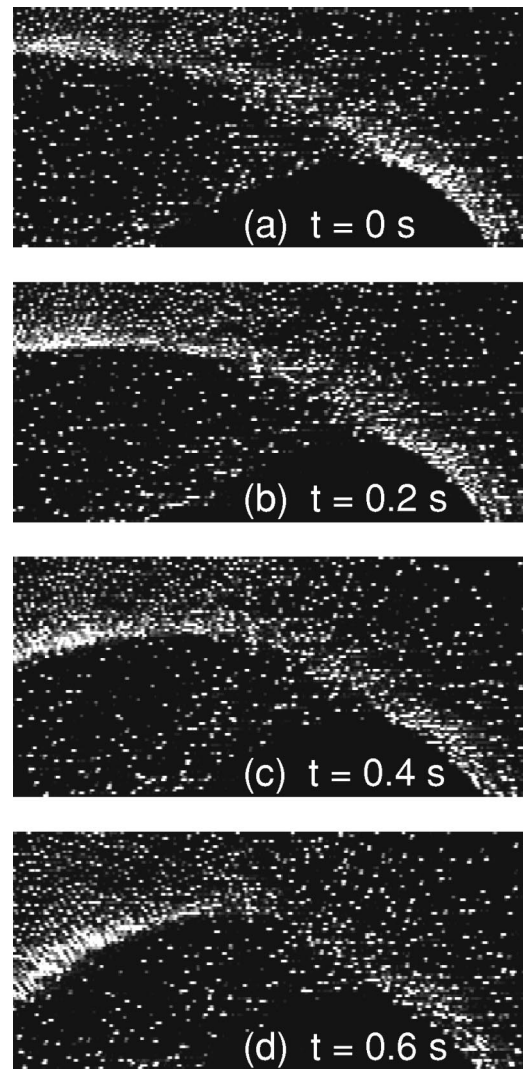


FIG. 3. Consecutive images of the shock wave taken at equal time intervals. The shock propagates from top to bottom in the left upper part of the frame. The shown cropped field of view is  $15 \times 6.7$  mm.

ticle positions and tracing them from one frame to the next. This allowed us to calculate the particle velocities. The particle number density was calculated by counting the number of particles in a known volume of space, taking into account that the thickness of the illuminating laser sheet was  $80 \pm 20 \mu\text{m}$ . This uncertainty introduces a systematic error of  $\pm 25\%$ .

In order to reduce the statistical uncertainty the data was averaged in bins. Figure 4 illustrates how the bins were formed and labeled. We identified three points on the front in every frame. The point on the right was a natural choice since it does not move—the front rotates around it. Two other points are equidistant. The points were fitted with a parabola, which was then shifted up and down to form the bin boundaries parallel to the curved shock. A normal to the parabola was drawn at the midpoint. Lines parallel to this normal formed the other bin boundaries.

To characterize the motion of the perturbation front, we calculated the absolute value of the displacement for the midpoint of each bin (Fig. 5). One can see that the front

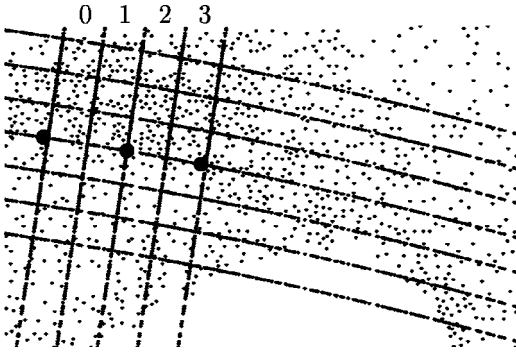


FIG. 4. Configuration of the bins used to average the particle number density and velocity. Three points (indicated with filled circles) are chosen on the shock front. They are fitted with a parabola. The bins are formed by parallel parabolas and normals to them.

velocity is not a constant. Slow initially, it accelerates at about 0.4–0.7 s (this time period was used for averaging of the quantities characterizing the perturbation) and then slows down again. Average velocities of the sections of the front are summarized in Table I, and the particle number density variation across the front is shown in Fig. 6. The number density is low in front of the perturbation and then increases sharply by a factor of 3. It is worth noting that the particle numbers in the region just behind the front are systematically undercounted. This leads to a corresponding underestimate number density at distances close to 0 in Fig. 6. This is illustrated by Fig. 7, which shows the magnified front at  $t = 0.6$  s. Particles at the very front move at about the speed of the shock and leave streaks, thus, masking other particles.

After about 0.55 s, the front has reached its greatest speed. There are two ways of measuring this. One is from the displacements shown in Fig. 5, the other from the length of the streaks of the particles at the front. The former yields a speed of about 0.85 cm/s and latter about 1.0 cm/s. Note that particle trajectory superposition can only lead to a larger value than the correct velocity, so that the 1.0 cm/s is regarded as an upper limit.

### III. DISCUSSION OF RESULTS

We may estimate the dust-acoustic wave speed from [16]

$$v_{DAW}^2 = \frac{k_B T_d}{m_d} + \frac{k_B T_i}{m_d} \frac{P Z_d}{1 + P + \tau}, \quad (1)$$

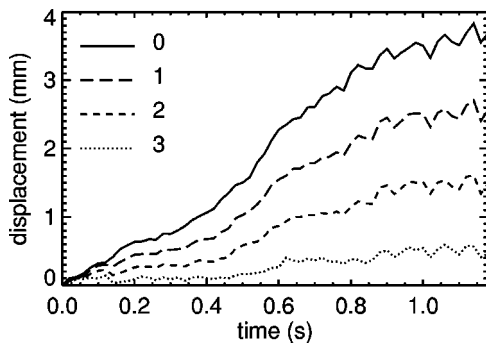


FIG. 5. Average displacements of the shock front sections corresponding to different bins.

TABLE I. Average speed of the shock front corresponding to different bins.

Bin number	0	1	2	3
Speed (mm/s)	5.3(±19)%	3.7(±32)%	2.2(±54)%	0.95(±57)%

where  $P = n_d Z_d / n_e$  is the Havnes parameter,  $\tau = T_i / T_e$  is the ratio of ion and electron temperature,  $Z_d$  is the dust equilibrium charge. Using measured quantities ahead and behind the perturbation front, we determine the complex plasma conditions as given in Table II. From this, we derive the dust-acoustic wave speed to be 0.7 cm/s ahead of the perturbation front (and 0.95 cm/s behind it).

The uncertainty in this determination of  $v_{DAW}$  is much larger than the measurement uncertainty (which is only 10%). This is because the charge on the microparticles,  $Z_d$ , cannot be measured directly and because the ion density inside the complex plasma is uncertain due to recombination effects. We have calculated  $Z_d$  taking into account the different particle densities. In front of the perturbation, we get  $Z_d = 4 \times 10^3$  and behind it  $Z_d = 3.3 \times 10^3$ . Also we took  $n_i = 2 \times 10^9 \text{ cm}^{-3}$  in accord with the previous measurements and numerical simulation models. Our values for  $v_{DAW}$  are also in accord with the results obtained by Khrapak *et al.* [17] from another experiment conducted with PKE-Nefedov.

Taking these values with all due caution, it appears possible that the traveling perturbation front may have steepened and speeded up to form a weak dust-acoustic shock, with Mach number  $1 \leq M_{DA} \leq 1.4$ . So from now on we will refer to the front as a “shock”—at least during the time interval 0.4–0.6 s (fully aware that it might not have reached the shock phase at all) and investigate it kinetically.

The shock front has a “microroughness,” when viewed at the kinetic level. This is an interesting quantity to determine, because it has different meanings for different shocks. For instance, in a gas dynamic shock, the shock thickness is  $l_s \approx \nu / c_s$ , where  $\nu \approx \lambda c_s$  is the kinematic velocity,  $c_s$  is the sound speed, and  $\lambda$  is the mean free path of the particles. This gives  $l_s \approx \lambda$ . In a low Mach number plasma shock  $l_s \approx 2\pi / k_s$ , where  $k_s$  is the wave number at which the phase

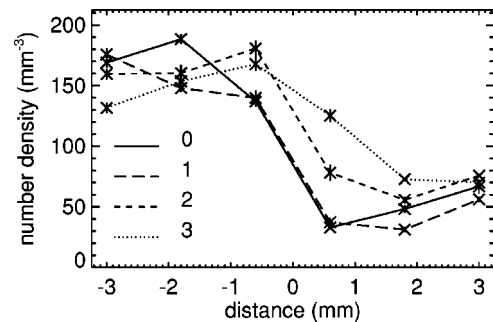


FIG. 6. Particle number density across the shock. The shock front is positioned at zero distance and propagates in the positive direction. The number density is lower in front of the shock and about three times higher behind it.

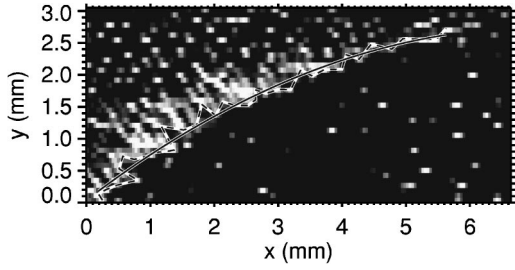


FIG. 7. Magnified shock front at time  $t = 0.6$  s. The particles in the narrow region ( $\approx 0.5 - 1$  mm) at the front move at a speed close to the speed of the shock front. The speed can be determined from the length of the particle tracks and from following the particles in consecutive video images. The dashed line shows the shock front, while the solid line indicates a parabolic fit. The shock front is characterized by a roughness parameter  $l_r = 0.17$  mm, which is close to the particle separation  $a = 0.19$  mm

velocity of ion whistler waves ( $\omega/k$ ) equals the shock speed  $v_s$ . This yields  $l_s \approx 2\pi\lambda_i(M^2 - 1)^{-1/2}$ , where  $M$  is the Mach number and  $\lambda_i = c/\omega_p$  is the ion inertial length ( $\omega_p$  is the plasma frequency).

There is another clan of shocks, which develop a precursor due to the production of fast waves or energetic particles, which travel ahead of the shock and signal its arrival by depositing their momentum in the upstream medium. The typical shock structures that are obtained in such situations are of the order of the damping length of such waves or the typical transport (e.g., diffusion) length scales  $\kappa/v_s$ , where  $\kappa$  is a spatial diffusion coefficient. In complex plasmas, any of these situations could occur. There are fast wave modes in addition to the basic dust-acoustic wave (e.g., the dust-ion acoustic wave). In the strong coupling state, the system may behave like a classical fluid (except that the interaction potentials are different). In weaker coupling states it may behave like a plasma (with the dust-acoustic wave playing the role of the ion-acoustic wave).

Hence investigating the shock thickness or microroughness kinetically helps us to identify the generic thermodynamic state of the complex plasma.

The microroughness was determined by manually selecting the particles on the front boundary and connecting them with a line (dashed line in Fig. 7). We fitted this line with a parabola (solid line in Fig. 7) to approximate the shock front. The area  $A$  between the front boundary and the parabolic fit was computed in order to characterize the shock roughness.

Assuming that the bumps on the boundary have triangular shape, we estimated the roughness parameter as  $l_r = 2A/l = 0.17$  mm, where  $l$  is the length of the fit to the shock front. Assuming a sequence of  $N$  equilateral triangles with height  $h_i$  and base  $x_i$ , the roughness parameter becomes

$$l_r = \frac{\sum_{i=1}^N h_i x_i}{\sum_{i=1}^N x_i}, \quad (2)$$

i.e., it gives an approximately kinetically averaged shock thickness. The measured value or  $l_r$  is very close to the particle separation  $a = n_d^{-1/3} = 0.19$  mm, where  $n_d$  is the dust number density.

Let us consider the complex plasma in a light of the previous comments. In complex plasmas, the electrostatic collision cross section is  $\sigma \approx \pi\lambda_{Di}^2$ —the square of the Debye length. This is due to shielding. The mean free path of the particles is then  $\lambda_c \approx 1/(n\pi\lambda_{Di}^2)$ . Using the figures from Table II and substituting  $1/n = (\kappa\lambda_{Di}^2)$  we get  $\lambda_c \approx \kappa^3\lambda_{Di}/\pi = 0.13$  cm or  $\lambda_c \approx 7a$ . This is substantially larger than the measured microroughness, suggesting that collisions, analogous to a gas shock, are not a determining factor.

Alternatively, treating the complex plasma analogously to ordinary two component plasmas, we obtain a shock thickness

$$l_{ds} = \frac{2\pi v_{DAW}}{\omega_{dp}\sqrt{M^2 - 1}} \approx 0.26 \text{ mm}$$

for  $M = 1.3$ , which is much closer to the observed value.

Finally, we need to consider another damping mechanism, which will slow down “fast” particles that might escape from the front upstream—neutral gas drag. Using the Epstein formula, we get a stopping length  $l_E = v_s\tau_E = 0.08$  mm. This result suggests that neutral gas drag can indeed slow down “runaway” particles in a very short distance indeed, causing a short scale size for any disturbance. However, this damping should also work in the backward direction behind the shock—essentially making the accelerated particles stationary again after a distance  $l_E$ . In other words, the pulse width is roughly 10 times larger, 0.8 mm. This suggests that the Epstein drag law used, which applies to isolated test particles, may not be appropriate in strongly coupled complex plasmas—most likely due to collective effects. In this case, Coulomb collisions amongst the particles can become the

TABLE II. Plasma conditions at the perturbation front. Only errors due to the uncertainty in the particle density measurements have been considered. The ion density was taken to be  $2 \times 10^9 \text{ cm}^{-3}$ , the electron temperature 1 eV, and the microparticle temperature in front of the perturbation was the same as the neutral gas temperature  $T_1 \approx 300$  K.

Parameter	In front of the shock	Behind the shock
$\Gamma = (Z_d^2 e^2 / aT) \exp[-(a/\lambda_{Di})]$	3.7 ( $\pm 70\%$ )	$(T_1/T_2)43 (\pm 45\%)$
$\kappa = a/\lambda_{Di}$	6.8 ( $\pm 6\%$ )	4.7 ( $\pm 6\%$ )
$a (\mu\text{m}) = n_d^{-1/3}$	270 ( $\pm 6\%$ )	188 ( $\pm 6\%$ )
$\omega_{dp} (s^{-1}) = (4\pi n_d Z_d^2 e^2 / m_d)^{1/2}$	$2.7 \times 10^2 (\pm 10\%)$	$4.6 \times 10^2 (\pm 10\%)$

determining factor again, i.e.,  $\lambda_c$  would be the appropriate length scale or some intermediate value between  $\lambda_c$  and  $\lambda_E$ . The angular spread in the particle trajectories behind the front supports this.

Finally, we need to address another point: the plasma potential varies in a complex plasma across a density jump [11]. For the situation we have here (with ion density, electron temperature, etc., as mentioned earlier), the Havnes parameter changes from  $P=0.1$  in front to  $P=0.25$  behind the shock. This leads to a potential drop of 0.8 V across the shock front, which adjusts itself “instantaneously” with respect to the time scales of interest here. It is this potential, which accelerates and “sweeps up” the upstream particles.

The final velocity of the shock is given by the modified Rankine-Hugoniot equations taking into account the strong coupling. These are the continuity equation

$$n_1 u_1 = n_2 u_2, \quad (3)$$

and the energy conservation equation

$$m n_1 u_1^2 - m n_2 u_2^2 = P_2 - P_1, \quad (4)$$

with the pressures given by

$$P_1 = (\Gamma_1 + 1) n_1 k_B T_1, \quad (5)$$

$$P_2 = (\Gamma_2 + 1) n_2 k_B T_2, \quad (6)$$

where the subscript 1 denotes the region ahead of the shock and 2 denotes the region immediately behind it. Substituting from the measurements and from the derivations of Table II, we end up with the result that the dust-acoustic Mach number is  $1.20 \leq M_{DA} \leq 1.34$ . Thus the analysis is (at least) self-consistent and supports the notion that the perturbation has steepened up into a weak dust-acoustic shock.

#### IV. SUMMARY

In summary, we were able to excite a traveling discontinuity in a complex plasma under microgravity conditions.

(Microgravity is important for this kind of measurement, because external body forces are approximately two orders of magnitude smaller than interparticle forces, making the system very homogeneous.) This discontinuity speeded up and steepened, which suggested that it might have been developing into a dust-acoustic shock as it propagated into the less dense medium. Analysis revealed that it might indeed be a weak shock with dust-acoustic Mach number of around 1.2–1.4. The shock is extremely sharp, with a microroughness scale of the same order as the interparticle separation and the compressed region behind the shock extends to about 10 times the stopping length calculated for neutral gas drag. The latter is probably due to collective phenomena and dominated by isotropising Coulomb collection. A simple modified Rankine-Hugoniot condition was used, which includes the Coulomb pressure of the strong coupling, to check the results. It could be shown that they were internally consistent, reinforcing the conclusions about the identification of a dust-acoustic shock.

#### ACKNOWLEDGMENTS

This work was supported by DLR/BMBF under Grant No. 50WM9852. The authors wish to acknowledge the excellent support from the PKE-Nefedov Team (see below) and the agencies involved in making PKE-Nefedov a success: DLR, Rosavia-Cosmos, Ministry of Industry, Science and Technologies of the Russian Foundation for Basic Research, TSUP, RKK-Energia, Kayser-Threde, TSPK, IPSTC, and the cosmonauts. The PKE-Nefedov team (in alphabetical order): M. Belyaev, H. Binnenbruck, V. Blagov, L. Deputatova, V. Fortov, J. Goree, S. Goryainov, Y. Grigoriev, W. Griethe, T. Hagl, A. Ivanov, A. Kellig, R. Klett, C. Korner, U. Konopka, M. Kudashkina, R. Kuhl, S.Kusnetsov, A. Lebedev, A. Lipaev, V. Molotkov, G. Morfill, A. Nefedov, V. Nikitsky, O. Petrov, H. Pfeuffer, M. Pronin, I. Roslavytzeva, T. Rostopirov, M. Roth, H. Rothermel, P. Saburov, G. Schmidt, Y. Semenov, A. Sherbak, A. Shurov, H. Thomas, and M. Zuzic.

- 
- [1] J. Bond, K. Watson, and J. Welch, *Atomic Theory of Gas Dynamics* (Addison-Wesley, Reading, MA, 1965).
- [2] R. Graham, *Solids under High-Pressure Shock Compression* (Springer-Verlag, New York, 1993).
- [3] S. Hørluck and P. Dimon, *Phys. Rev. E* **60**, 671 (1999).
- [4] F. Chen, *Introduction to Plasma Physics and Controlled Fusion* (Plenum Press, New York, 1984).
- [5] R.Z. Sagdeev, *Reviews of Plasma Physics* (Consultants Bureau, New York, 1966), Vol. 4, pp. 23–91.
- [6] H.K. Andersen, N. D’Angelo, and P. Michelsen, *Phys. Fluids* **11**, 606 (1968).
- [7] N. Rao, P. Shukla, and M. Yu, *Planet. Space Sci.* **38**, 543 (1990).
- [8] N. Rao, *Planet. Space Sci.* **41**, 21 (1993).
- [9] F. Melandsø and P. Shukla, *Planet. Space Sci.* **43**, 635 (1995).
- [10] S.I. Popel, M.Y. Yu, and V.N. Tsytovich, *Phys. Plasmas* **3**, 4313 (1996).
- [11] O. Havnes, T. Aslaksen, T. Hartquist, F. Li, F. Melandsø, G. Morfill, and T. Nitter, *J. Geophys. Res., [Space Phys.]* **100**, 1731 (1995).
- [12] Y. Nakamura, H. Bailung, and P.K. Shukla, *Phys. Rev. Lett.* **83**, 1602 (1999).
- [13] Q.-Z. Luo, N. D’Angelo, and R.L. Merlino, *Phys. Plasmas* **6**, 3455 (1999).
- [14] D. Samsonov, J. Goree, H.M. Thomas, and G.E. Morfill, *Phys. Rev. E* **61**, 5557 (2000).
- [15] G. Morfill, H. Thomas, U. Konopka, H. Rothermel, M. Zuzic, A. Ivlev, and J. Goree, *Phys. Rev. Lett.* **83**, 1598 (1999).
- [16] V.N. Tsytovich, U. de Angelis, and R. Bingham, *Phys. Rev. Lett.* **87**, 185003 (2001).
- [17] S. Khrapak, D. Samsonov, G. Morfill, H. Thomas, V. Yaroshenko, and PKE-Nefedov team, *Phys. Plasmas* **10**, 1 (2003).